An empirical model of noise sources in subsonic jets, formulated in a linear resolvent framework

Ugur Karban, Benjamin Bugeat, Anurag Agarwal, Lutz Lesshafft, Peter Jordan

An empirical model of noise sources in subsonic jets, formulated in a linear resolvent framework

Ugur Karban*
Middle East Technical University, 06800, Ankara, Turkey

Benjamin Bugeat † and Anurag Agarwal‡
University of Cambridge, Cambridge, CB2 3AP, United Kingdom

Lutz Lesshafft§
CNRS - École Polytechnique, 91128, Palaiseau Cedex, France

Peter Jordan¶
Institut Pprime, CNRS-Université de Poitiers-ENSMA, 86962 Chasseneuil du Poitou, France

We present an analysis aiming to identify the acoustically efficient forcing components in subsonic jets using an LES database. The forcing terms, which correspond to the source terms in the classical terminology of acoustic analogies, are defined within the resolvent framework. We extract from a jet database at Mach number, $M = 0.4$, which contains both state and forcing data, a low-rank representation of the acoustic field and a low-rank forcing that is correlated with it. We show that the forcing components that generate 99% of the acoustic energy in the downstream region correspond to less than 1% of the total forcing energy.

I. Introduction

Jet noise is one of the most studied subjects in aeroacoustics since the first work by Lighthill [1]. Developing models for turbulent noise prediction that are accurate enough and may finally lead to design of mitigation strategies is still an active research topic even for the simplest flows despite the substantial literature on the field over the last 70 years. The fundamental problem making turbulent noise prediction so difficult is that the Navier-Stokes (N-S) equations do not include separate mechanisms to generate fluctuations propagating across the flow domain from those to create local perturbations convected by the flow. It is therefore not possible to uniquely define the acoustic sources and sound generation/propagation mechanisms in a given turbulent flow.

Lighthill attacks this problem by rearranging the Navier-Stokes (N-S) in wave equation form assuming quiescent medium, and considering the terms left outside the wave equation as acoustic sources, which is called Lighthill's acoustic analogy [1]. His work is followed by many other analogies in the literature (Powell [2], Phillips [3], Lilley [4], Howe [5], Doak [6], Goldstein [7]). The general idea underlying in acoustic analogies is that one chooses an acoustic variable and a linear propagator for the acoustic waves. The source is then defined, once the N-S equations are rearranged to include the linear propagator, as the terms that the linear propagator do not apply on. This provides splitting sound generation and propagation given a turbulent flow.

One can alternatively use the resolvent analysis (McKeon and Sharma [8], Hwang and Cossu [9]) to handle this splitting problem. Resolvent analysis involves linearising the N-S equations around the mean flow, and re-arranging them in input-output form, or as frequently used in resolvent terminology, forcing-response form. The response can be defined flexibly as any part of the state and the forcing consists of the nonlinear fluctuating terms that remain after linearisation around the mean. A property to be noted about the resolvent analysis, and also the acoustic analogies, is that it is exact in the sense that if one has access to the forcing and mean-flow data with great accuracy, it yields the exact response. Having a DNS database, for instance, one can construct a resolvent framework, in which the forcing terms generate the response including the acoustic pressure, i.e., the pressure field outside the region of hydrodynamic activity.

*Post-doctoral research fellow, Department of Aerospace Engineering, Universiteler Mh., Dumlupinar Blv. 1/6 D:133
†Post-doctoral research fellow, Department of Engineering, Trumpingtion Street
‡Professor, Department of Engineering, Trumpington Street
§Research Director, Laboratoire d'Hydrodynamique.
¶Research Director, Départment Fluides Thermique et Combustion, 11 Boulevard Marie et Pierre Curie.

Such an exactitude, however, is not very useful by itself in terms of modeling the mechanisms behind response generation. Turbulence, when described in a linear framework such as resolvent analysis, can be considered mostly a suboptimal system. The state is usually generated as residuals of significant cancellations between different forcing structures. Or in certain cases, some part of the forcing can be silent, i.e., it is filtered via the resolvent operator such that no response is generated. These two concepts apply to noise generation in turbulent jets as well. Having silent or inefficient forcing structures next to *active* structures that actually drive the acoustic field makes crucial to develop strategies for source identification in turbulent flows.

Using a linear operator that takes into account all the linear amplification and scattering mechanisms can be crucial to simplify the source terms. However, for subsonic jets, using a model that depends only on the linear amplification mechanism contained in the resolvent operator is not sufficient to predict the noise with good accuracy [10]. Such linear models should be coupled with the effect of the jitter mechanism resulting in coherence decay observed in wavepackets in subsonic jets [11, 12].

Developing a source model taking into account these nonlinear jitter effects for a range of operating conditions is the main objective of this study. We focus on the axisymmetric sound generation at low propagation angles which is known to be dominant part of the overall noise generated by isolated subsonic jets [10, 13]. We employ resolvent analysis to achieve the splitting between sound generation and propagation. Spectral proper orthogonal decomposition (SPOD) method [14–17] is used to obtain a low-rank description of aft-angle jet noise. We also use a method called resolvent-based extended SPOD (RESPOD) [18] to extract the associated low-rank forcing terms. The resolvent operator connects low-rank source terms obtained by RESPOD to the low-rank acoustic field obtained using SPOD. This analysis is systematic, i.e., can be applied to any flow with any particular response in focus. An implementation on wall-bounded flows was shown in Karban et al. [18]. With further inspection of these low-rank sources in terms of the acoustic matching criterion [19–21], we identify the parts that actively generate the sound at low angles.

The structure of the paper is as follows: the mathematical framework for resolvent analysis and RESPOD method is revisited in §II. The details about the numerical database and the tool to perform resolvent analysis are given in §III. The process to identify forcing components that generate downstream jet noise is explained in §IV. Finally, some concluding remarks are provided in §V.

II. Modelling framework

A. Governing equations in resolvent form

The compressible Navier-Stokes (N-S) equations are given in a compact form as,

$$\partial_t \mathbf{q} = \mathcal{N}(\mathbf{q}), \tag{1}$$

where $\mathbf{q} = [\nu\, u_x\, u_r\, u_\theta\, p]^\top$ is the state vector with ν and p, the specific volume and the pressure, respectively, and $\mathbf{u} = [u_x\, u_r\, u_\theta]^\top$, the velocity vector in cylindrical coordinates, where x, r and θ refer, respectively, to streamwise, radial and azimuthal directions, and $\mathcal{N}$ denotes the nonlinear N-S operator. All variables are non-dimensionalised by the ambient speed of sound, c_∞, density, ρ_∞, and the nozzle diameter, D. We consider a discretised system in space, for which linearisation around the mean, $\overline{\mathbf{q}}$, yields

$$\partial_t \mathbf{q}' - \mathbf{A}\mathbf{q}' = \mathbf{f}, \tag{2}$$

where prime denotes fluctuations around the mean, $\mathbf{A} = \partial_q \mathcal{N}|_{\overline{\mathbf{q}}}$ is the linear operator obtained from the Jacobian of $\mathcal{N}$ and $\mathbf{f}$ denotes all the remaining nonlinear terms, which is referred to henceforth as the forcing terms. In resolvent framework, Eq. (2) is Fourier transformed and rearranged to obtain

$$\hat{\mathbf{q}} = \mathbf{R}\hat{\mathbf{f}}, \tag{3}$$

where the hat indicates Fourier transformed quantities and $\mathbf{R} = (i\omega\mathbf{I} - \mathbf{A})^{-1}$ is the resolvent operator. The resolvent operator can be modified to focus on a particular measurement, instead of the full state, which can be defined as any linear transformation of the state vector, as;

$$\hat{\mathbf{y}} = \mathbf{C}\hat{\mathbf{q}}, \tag{4}$$

$$\hat{\mathbf{y}} = \tilde{\mathbf{R}}\hat{\mathbf{f}}, \tag{5}$$

where $\mathbf{C}$ denotes the measurement matrix and $\tilde{\mathbf{R}} \triangleq \mathbf{CR}$ is a modified resolvent operator. Throughout this paper, we will focus on the pressure in the acoustic field as our measured quantity, therefore

$$\mathbf{C} = [0\,0\,0\,0\,\alpha], \tag{6}$$

where $\alpha = 0$ in the near-field so as to suppress hydrodynamic fluctuations, and 1 in the acoustic field.

It is also possible to limit forcing by introducing another matrix, $\mathbf{B}$ on $\hat{\mathbf{f}}$ in Eq. (3), yielding

$$\hat{\mathbf{y}}_B = \tilde{\mathbf{R}}\mathbf{B}\hat{\mathbf{f}}. \tag{7}$$

Note that depending on the measured quantity, $\hat{\mathbf{y}}$, and the control matrix, $\mathbf{B}$, the condition,

$$\hat{\mathbf{y}}_B = \hat{\mathbf{y}} \tag{8}$$

may or may not be satisfied. Different $\mathbf{B}$ matrices will be employed to identify irrelevant forcing components for jet-noise problem, i.e., those terms which, when suppressed by $\mathbf{B}$, do not violate Eq. (8).

B. Resolvent-based extended spectral proper orthogonal decomposition

We want to obtain a low-rank representation of the acoustic field field and extract the associated low-rank forcing. A detailed discussion on how to achieve this for any measured flow quantity was provided in Karban et al. [18], where a method referred to as 'Resolvent-based Extended Spectral Proper Orthogonal Decomposition' (RESPOD) was used. RESPOD is based on the extended proper orthogonal decomposition presented by Borée [22] and is related to spectral proper orthogonal decomposition (SPOD) [14–17]. The aim in RESPOD is to find a forcing mode, $\boldsymbol{\chi}^{(p)}$, that is correlated with the p^{th} SPOD mode, $\boldsymbol{\psi}^{(p)}$, of the measured response, $\hat{\mathbf{y}}$. It was first presented in Towne et al. [23] and later discussed in Karban et al. [18] to identify the forcing structures that generate wall-attached eddies. Here, we briefly review the method highlighting how it can be adapted to find the low-rank forcing subspace associated with sound generation.

For a given ensemble of realizations $\hat{\mathbf{Y}} = [\hat{\mathbf{y}}_1 \cdots \hat{\mathbf{y}}_P]$ of an N dimensional discretised system where P is the number of Fourier realizations, SPOD involves eigen-decomposition of the CSD matrix $\hat{\mathbf{S}} \triangleq \hat{\mathbf{Y}}\hat{\mathbf{Y}}^H$,

$$\hat{\mathbf{S}} = \hat{\boldsymbol{\Psi}}\hat{\boldsymbol{\Lambda}}\hat{\boldsymbol{\Psi}}^H, \tag{9}$$

where the eigenmodes, $\hat{\boldsymbol{\Psi}}$, and eigenvalues, $\hat{\boldsymbol{\Lambda}}$, of $\hat{\mathbf{S}}$ are the SPOD modes and gains, respectively. An alternative way to obtain the SPOD modes, as shown in Towne et al. [16], is to perform an eigendecomposition of the system as,

$$\hat{\mathbf{Y}}^H\mathbf{W}\hat{\mathbf{Y}} = \hat{\boldsymbol{\Theta}}\hat{\boldsymbol{\Lambda}}\hat{\boldsymbol{\Theta}}^H, \tag{10}$$

where $\mathbf{W}$ is a positive-definite weight matrix, and $\hat{\boldsymbol{\Theta}}$ is a matrix containing the eigenmodes of $\hat{\mathbf{Y}}^H\mathbf{W}\hat{\mathbf{Y}}$. The eigenmodes, $\hat{\boldsymbol{\Psi}}$, and $\hat{\boldsymbol{\Theta}}$, are connected by,

$$\hat{\boldsymbol{\Psi}} = \hat{\mathbf{Y}}\hat{\boldsymbol{\Theta}}\hat{\boldsymbol{\Lambda}}^{-1/2}, \tag{11}$$

or alternatively as,

$$\hat{\boldsymbol{\Theta}} = \hat{\mathbf{Y}}^H\mathbf{W}\hat{\boldsymbol{\Psi}}\hat{\boldsymbol{\Lambda}}^{-1/2}. \tag{12}$$

Equation (11) indicates that it is possible to obtain the SPOD modes as a linear combination of the realizations. Writing (5) for the ensemble of realizations,

$$\hat{\mathbf{Y}} = \tilde{\mathbf{R}}\hat{\mathbf{F}}, \tag{13}$$

where $\hat{\mathbf{F}} \triangleq [\hat{\mathbf{f}}_1 \cdots \hat{\mathbf{f}}_P]$ is the matrix of forcing realisations, and multiplying (13) by $\hat{\boldsymbol{\Theta}}\hat{\boldsymbol{\Lambda}}^{-1/2}$, we get

$$\hat{\boldsymbol{\Psi}} = \tilde{\mathbf{R}}\hat{\mathbf{F}}\hat{\boldsymbol{\Theta}}\hat{\boldsymbol{\Lambda}}^{-1/2}. \tag{14}$$

Equation (14) can be written for the p^{th} SPOD mode by extracting the corresponding columns in the matrices, $\hat{\boldsymbol{\Psi}}$, $\hat{\boldsymbol{\Theta}}$ and $\hat{\boldsymbol{\Lambda}}$ as,

$$\hat{\boldsymbol{\psi}}^{(p)} = \tilde{\mathbf{R}}\hat{\mathbf{F}}\hat{\boldsymbol{\theta}}^{(p)}\lambda^{(p)^{-1/2}}, \tag{15}$$

where $\hat{\boldsymbol{\theta}}^{(p)}$ denotes the p^{th} column in $\hat{\boldsymbol{\Theta}}$ and $\lambda^{(p)}$ denotes the p^{th} diagonal element in $\hat{\boldsymbol{\Lambda}}$. We then define the RESPOD mode of forcing, $\hat{\boldsymbol{\chi}}^{(p)}$, as,

$$\hat{\boldsymbol{\chi}}^{(p)} \triangleq \hat{\mathbf{F}}\hat{\boldsymbol{\theta}}^{(p)}\lambda^{(p)^{-1/2}}. \tag{16}$$

Following Borée [22], it can be shown that the RESPOD mode, $\boldsymbol{\chi}^{(p)}$, contains all the forcing components correlated with the SPOD mode, $\boldsymbol{\psi}^{(p)}$. Furthermore, (15) indicates that the two modes are connected via the resolvent operator.

The ability to identify a RESPOD mode of the forcing with each SPOD mode of the response implies, for the jet-noise problem, that one can use this approach to identify the low-rank forcing subspace that is correlated with the low-rank sound field, and which, furthermore, generates the low-rank sound field when applied to the resolvent operator.

III. Numerical database and resolvent analysis tool

The numerical database used in this study consists of large eddy simulation (LES) of a subsonic, isothermal, ideally expanded jet at jet Mach number, $M_j \triangleq U_j/c_j = 0.4$ using the unstructured flow solver 'Charles' [24]. The database was validated against experimental data in Brès et al. [25], where detailed information about the database can also be found. The database consists of the state and the forcing data to be able to perform resolvent analysis. The forcing data, once the state data is stored, is obtained via the procedure devised in Towne [26] and summarised in the following:

1) Calculate the state $\mathbf{q}$ through LES at $dt = 0.001$, and store it at every 200^{th} time step.
2) Calculate and save the mean flow $\bar{\mathbf{q}}$.
3) Calculate and save $\mathcal{G}(\bar{\mathbf{q}})$, where $\mathcal{G}$ is the nonlinear LES operator. Note that $\mathcal{G}$ is different from the N-S operator, $\mathcal{N}$, as the sub-grid scales are filtered in $\mathcal{G}$.
4) For each snapshot, calculate $\partial\mathbf{q}/\partial t = \mathcal{G}(\mathbf{q})$.
5) For each snapshot, calculate $\mathbf{Aq}' \approx \frac{\mathcal{G}(\bar{\mathbf{q}}+\epsilon\mathbf{q}')-\mathcal{G}(\bar{\mathbf{q}})}{\epsilon}$, where ϵ is a sufficiently small number.
6) Interpolate $\mathbf{q}$, $\partial\mathbf{q}/\partial t$, and $\mathbf{Aq}'$ data on the cylindrical grid.
7) Compute forcing in time domain using (2).

Both the state and forcing data is Fourier transformed using blocks of 512 points in time with an overlap ratio of 75%. To minimize spectral leakage, an exponential windowing function [27] is used as,

$$W(t) = e^{n\left(4-\frac{T}{t(T-t)}\right)}, \tag{17}$$

with $n = 1$, and window size, $T = 512\Delta t$. The correction discussed in Martini et al. [27], which is necessary to satisfy (3) when windowing function is applied during the temporal Fourier transform (FT), is implemented while computing the forcing terms in the frequency domain.

Resolvent-based prediction of the response using the forcing data is achieved via a custom resolvent analysis code [28]. The code uses finite-volume method to solve linearised N-S equations decomposed into azimuthal Fourier modes. In this study, we focus on the axisymmetric part of the acoustic field, which is done by Fourier decomposing of Eq. (3) in the azimuthal direction and then investigating the first azimuthal mode. Since the mean flow in jets is axisymmetric, Eq. (3) can be written for a given azimuthal mode, m, as,

$$\hat{\mathbf{q}}^{(m)} = \mathbf{R}^{(0)}\hat{\mathbf{f}}^{(m)}, \tag{18}$$

where $\mathbf{R}^{(0)}$ denotes the axisymmetric part of $\mathbf{R}$. The response given in Eq. (18) is computed using the inverted system,

$$\mathbf{L}^{(0)}\hat{\mathbf{q}}^{(m)} = \hat{\mathbf{f}}^{(m)}, \tag{19}$$

where $\mathbf{L}$ is the sparse linear operator satisfying $\mathbf{L}^{-1} = \mathbf{R}$. The resolvent code solves the linear system of equations given in Eq. (19) via LU decomposition, using PETSc library [29]. Further details can be found in Bugeat et al. [28].

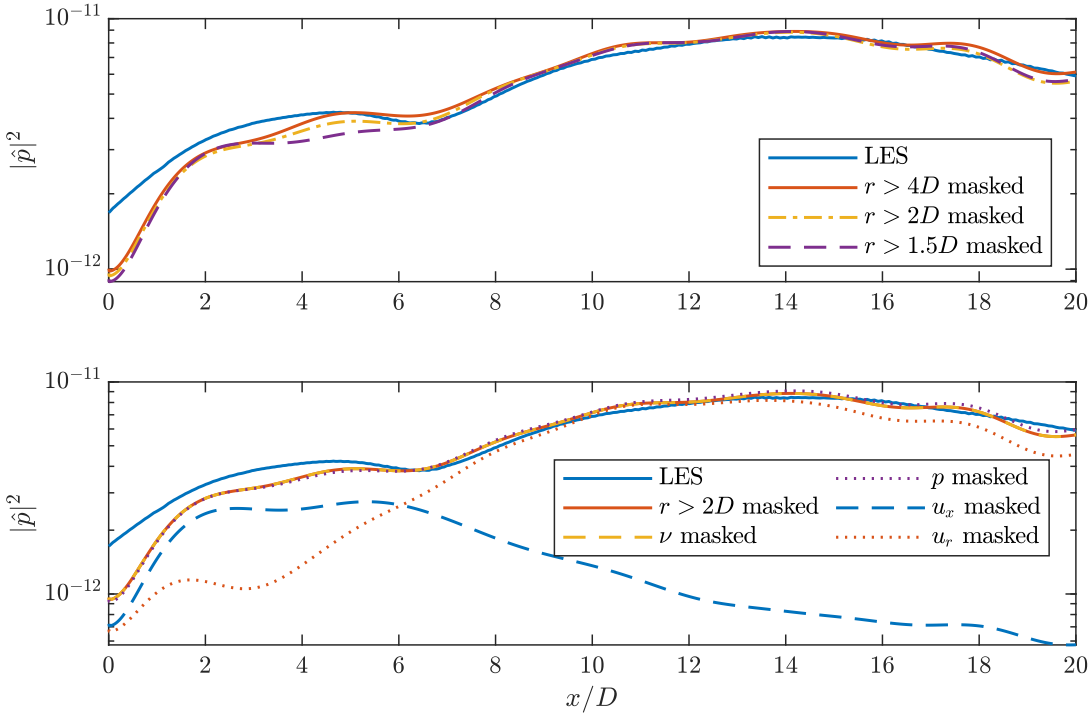

Fig. 1 PSD of pressure predicted using resolvent analysis with masking applied in space (top) and in variables (bottom) in comparison to the LES data at $r = 5D$ for the case M04Mc00 at $St = 0.6$.

IV. Identification of the acoustically efficient forcing components

In this section, we present a methodology based on the RESPOD framework outlined in §II, to identify the acoustically active forcing components, using the database, which contains both the state, $\mathbf{q}$, and the forcing, $\mathbf{f}$. We limit the study to mechanisms associated with noise generation at low polar angles, which we refer to as downstream noise. We then discuss how to further decompose the low-rank forcing associated to the acoustic field using acoustic matching criterion [19, 20]. In what follows, we present results for the frequency range, $St = [0.4, 1.0]$.

A. Masking the forcing vector

The forcing is modified using different $\mathbf{B}$ matrices to see the effect of spatial and componentwise masking. Figure 1 shows the effect of different masks on the acoustic pressure at $St = 0.6$. We see that masking the forcing beyond $r > 2D$ does not cause significant change in the acoustic pressure. Masking beyond $r > 1.5D$ yields a slight modification in the region, $x/D = [3, 6]$. We therefore consider the forcing in the region $r < 2D$ for the rest of the analysis.

Componentwise masking of the forcing shows that the components, f_ν and f_p, which correspond to the specific volume and the pressure, respectively, have negligible contribution to the sound field. The analysis also reveals that the forcing component in the radial direction, f_{u_r}, is mainly contributing to sideline noise, while the forcing component in the streamwise direction, f_{u_x}, is the main responsible for the downstream noise generation. These results are consistent with observation of Freund [30] using Lighthill's analogy. In what follows, focusing on the downstream noise generation only, we aim to identify the acoustically active subspace associated with this component alone.

B. Applying RESPOD method to obtain low-rank forcing

We are interested in obtaining a low-rank representation of the subspace of the forcing associated with the most-energetic components of the acoustic field. This requires first obtaining a low-rank representation of the acoustic field. We use SPOD for this purpose. In figure 2, the SPOD gains of the pressure in the downstream acoustic field, defined as $x/D, r/D \in [6, 30] \times [4, 6]$, and those of the forcing term, f_{u_x}, in the turbulent region, defined as

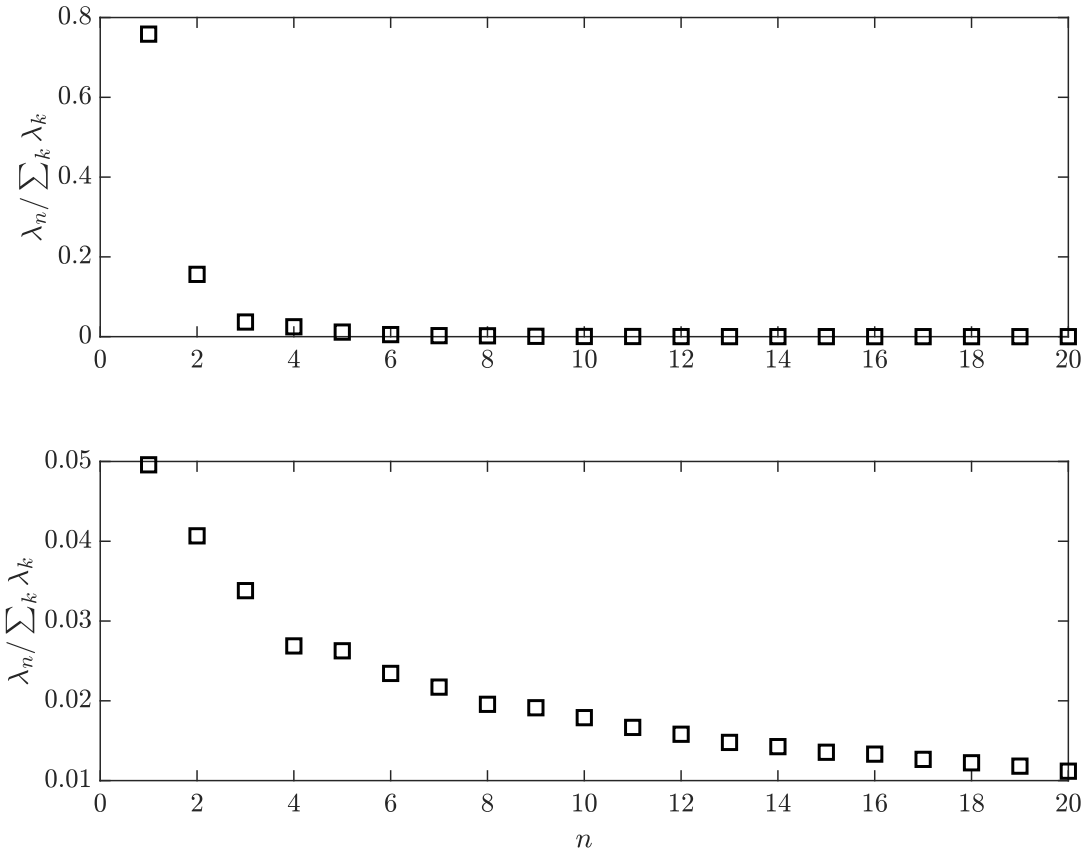

Fig. 2 SPOD gains of the pressure in the acoustic field (top) and streamwise forcing, f_{u_x} in the near field for the case M04Mc00 at $St = 0.6$.

$x/D, r/D \in [0, 30] \times [0, 2]$, are shown for $St = 0.6$. For the sound field, the leading SPOD eigenvalue corresponds to more than 75% of the total acoustic energy. The sum of the first five SPOD eigenvalues corresponds to 99% of the total acoustic energy, indicating a low-rank organisation in the acoustic field. For the forcing in the near field, on the other hand, we see that the leading SPOD mode contains less than 6% of the total energy in f_{u_x}. Around hundred modes are required to capture 90% of the total forcing energy, indicating an extremely high-rank structure.

Using RESPOD, we extract from this high-rank forcing data, a low-rank subspace that is correlated with the low-rank pressure structures observed in the acoustic field. In figure 3, we show the leading SPOD mode of pressure in the acoustic field, and the associated RESPOD mode of forcing in the near field, together with the energy distribution of the first twenty RESPOD forcing modes. The leading SPOD mode indicates the existence of a dominant oblique wave with constant propagation angle in the acoustic field. The associated forcing mode contains, although being much more disorganised compared to the acoustic mode, some wavy structures tilted in the direction of the mean flow, which has higher velocity in the jet center. We see that this first RESPOD mode contains less than 0.8% of the total forcing energy while it is associated with the leading SPOD mode of the acoustic field, corresponding to 75% of the total noise in the downstream region. This result shows how crucial is this identification step for a successful source modeling. Without this identification, an empirical model fitting the forcing data is most likely to be biased by the existence of energetic structures that do not contribute to sound generation.

No smooth trend is observed in the energy of the first twenty RESPOD forcing modes, contrary the SPOD modes in the acoustic field. This lack of smoothness in the RESPOD forcing mode gains suggest that these modes are underconverged, which is also the potential reason for the disorganised structures seen in the first RESPOD forcing mode. However, this under-convergence does not pose a problem in the following analysis. The SPOD modes of the response and the RESPOD modes of the forcing are computed using Fourier realisations of response and forcing that

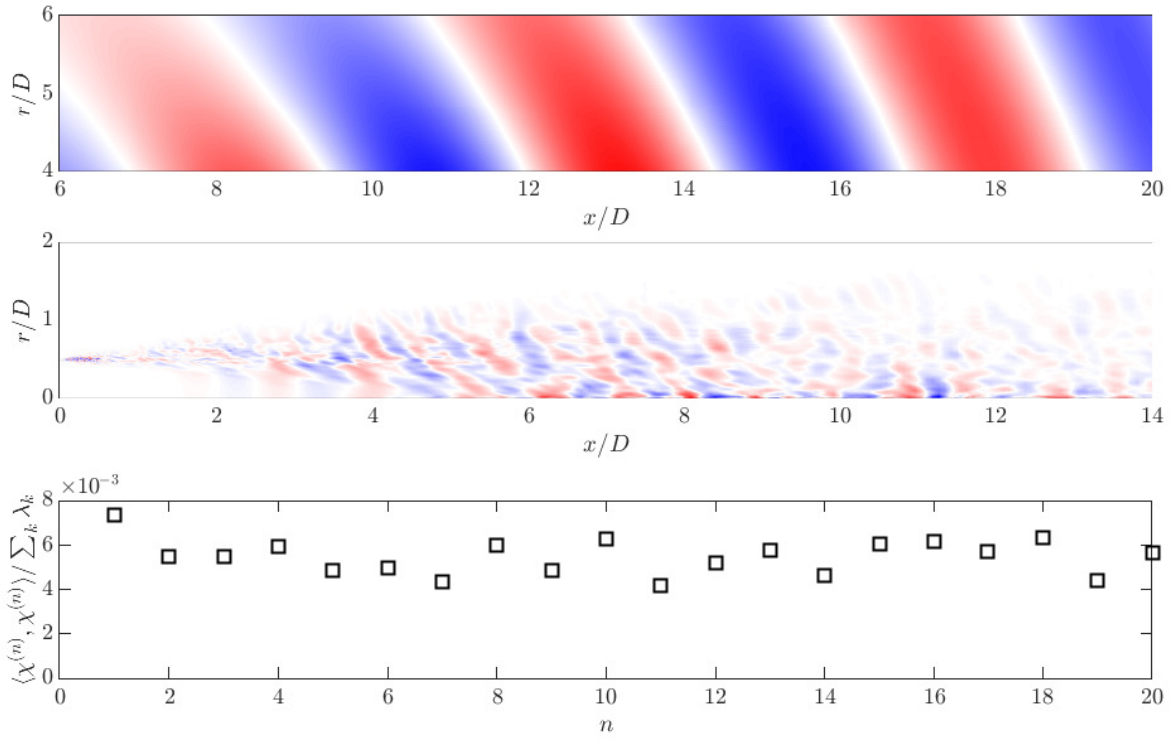

Fig. 3 Optimal SPOD mode of acoustic pressure (top) and the associated RESPOD mode of forcing (center) together with the energy distribution in the first twenty RESPOD modes of forcing (bottom) for the case M04Mc00 at $St = 0.6$**.**

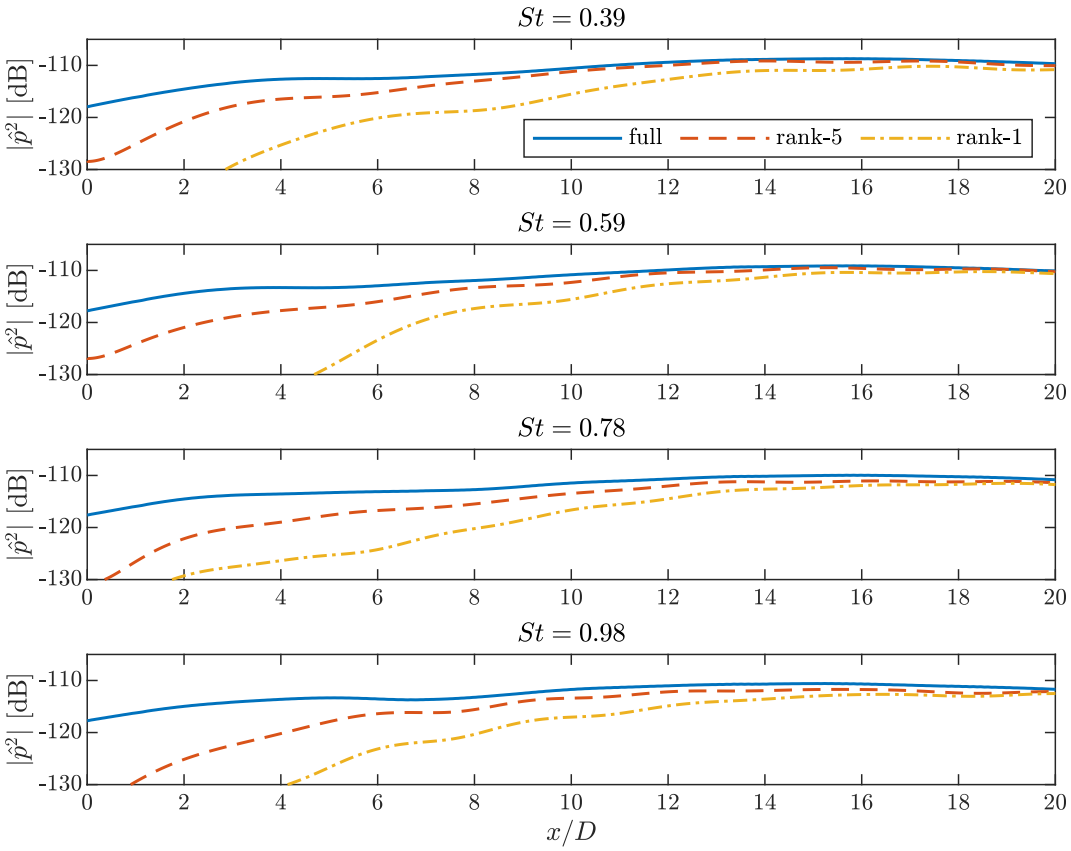

Fig. 4 PSD of acoustic pressure generated using rank-5 and rank-1 forcing, respectively, obtained by RESPOD, in comparison to acoustic field obtained from LES data (corresponding to full-rank forcing in the ideal case) at different frequencies ranging from $St = 0.4$ to 1 (from top to bottom).

exactly correspond to the same time instant. Eq. (3) is therefore satisfied for each pair of response-forcing realisations. This indicates that, no matter how under-converged the forcing data is, the structures generating the converged acoustic field are, by construction, ensured to be contained in the forcing mode seen in figure 3.

In figure 4, we show a comparison of the true acoustic field and the acoustic fields obtained using rank-5 and rank-1 forcing truncations obtained using RESPOD for a number of frequencies, $St \in [0.4, 1]$. We see that the rank-5 forcing recovers nearly the entire acoustic field in the downstream region. The rank-1 forcing also recovers a significant portion of the downstream acoustic field. It should be noted that although the acoustic field predicted by the rank-1 forcing should correspond to 75% of the total acoustic energy, the actual prediction amounts to less than this ratio. This is due to the errors contained in the LES database, causing a loss in the correlation information between the response and the forcing. These errors are originated from a number of reasons: interpolation errors, incompatibility between the resolvent code based on N-S equations and the LES data obtained by solving filtered N-S equations, and aliasing can be listed as dominant ones among other potential sources of error. Despite all the limitations of the existing database, we see that it is still possible to define a rank-1 forcing which can generate most of the downstream noise.

In what follows, we further decompose the rank-1 forcing obtained by RESPOD to extract the acoustically active forcing components which drive the leading SPOD mode of the acoustic pressure seen in figure 3.

C. Streamwise Fourier decomposition of the forcing

In figure 5, the acoustic fields generated by the first three RESPOD modes are shown at a number of frequencies, $St \in [0.4, 1.0]$. The first modes at all frequencies contain a single oblique wave with no jump in the phase. There exists on the other hand a line of phase shift in the second modes that moves upstream with increasing frequency. The phase

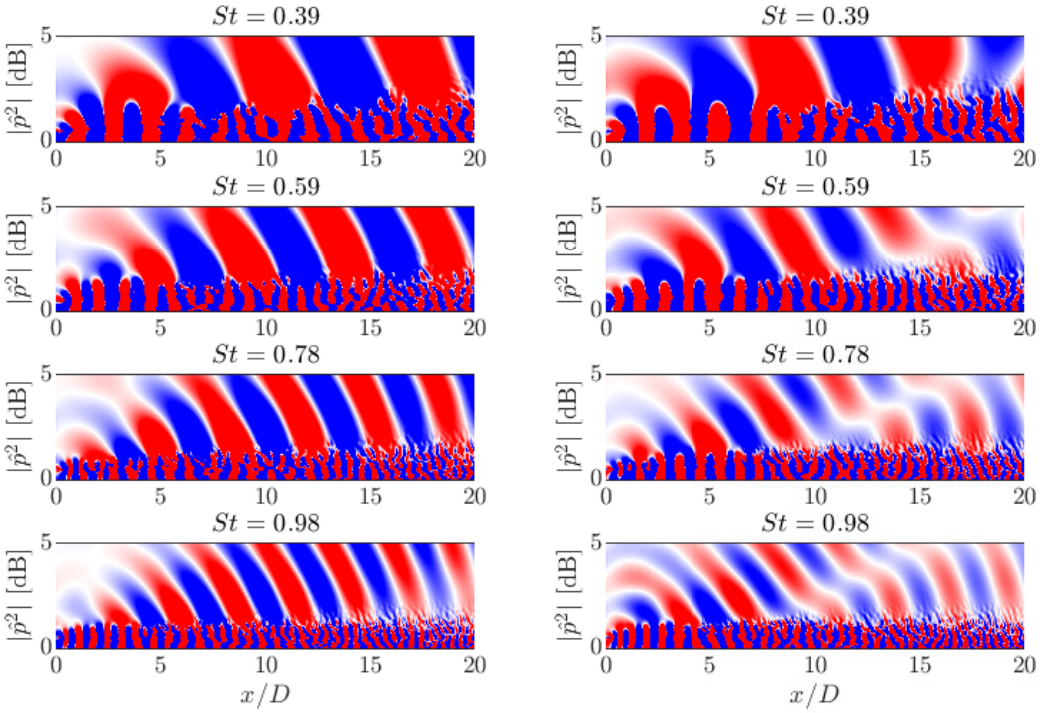

Fig. 5 Real part of pressure generated using first (left), and second (right) RESPOD mode of forcing at different frequencies ranging from $St = 0.4$ to 1 (from top to bottom). Color scale ranges between $[-1 \times 10^{-6}, 1 \times 10^{-6}]$.

shift appears in order to satisfy orthogonality between the first and the second modes, which is expected as RESPOD finds the forcing modes that generate the SPOD modes, which comprise an orthogonal basis. Note, however, that, no such orthogonality is ensured for the forcing modes.

The nearly constant propagation angle, which is roughly 30°, seen at all frequencies, is reminiscent of a Mach-wave-like mechanism (c.f. Tam et al. [13]). To explore this trend, we consider a wave in the streamwise direction defined by, $\exp(-ik_x x)$, where k_x is the streamwise wavenumber associated with a phase speed, c_x,

$$c_x = k_x \omega, \tag{20}$$

where ω is the angular frequency. In Mach-wave-like propagation, the phase speed is greater than the speed of sound, c_∞, and the propagation angle is given by $\cos^{-1}(c_\infty/c_x)$ [19, 20]. We project the first and the second RESPOD forcing modes onto this wave, varying in the phase speed over the range $[c_\infty,\ 2c_\infty]$, yielding,

$$a^{(p)}(k_x, St) = \langle \boldsymbol{\chi}^{(p)}(x, r, St), e^{-ik_x x} \rangle \triangleq \int_S \boldsymbol{\chi}^{(p)}(x, r, St) e^{-ik_x x} dS, \tag{21}$$

where p is the RESPOD mode number and S is 2D domain spanning the x and r directions. The results are shown in figure 6. It is seen that at all frequencies, the projection coefficient, $a^{(1)}$, peaks around 1.1-1.2c_∞, which corresponds to an angle of $\sim 30°$, consistent with the propagation angle observed in the acoustic response field. The coefficient, $a^{(2)}$, on the other hand, has a dip around the same value at all frequencies, reminiscent of the orthogonality observed in the response modes of figure 5.

These results suggest that projection of the forcing on to supersonic waves is the relevant mechanism for generation of downstream noise, consistent with previous hypotheses and models [10, 21, 30, 31]. To test this hypothesis, we define the following Fourier transform (FT) in the streamwise direction,

$$\mathcal{F}_x(\mathbf{a}) = \int_0^L \mathbf{a} e^{-ik_x x} dx, \tag{22}$$

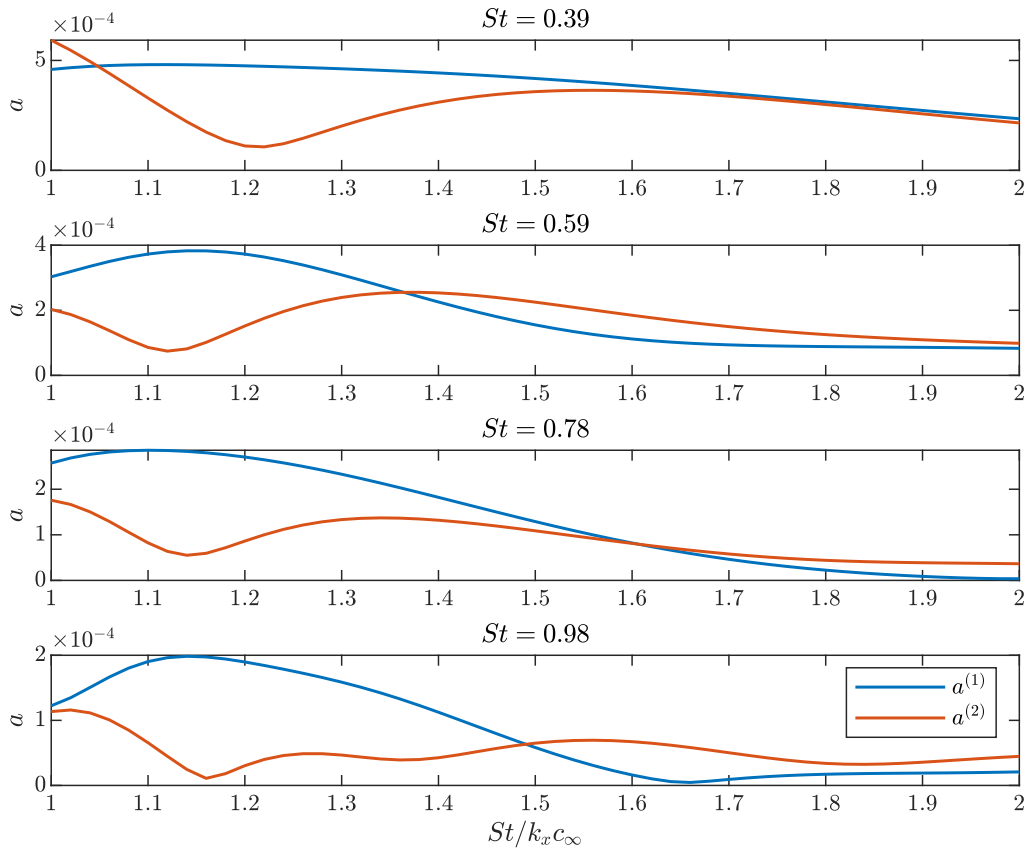

Fig. 6 Projection of first and second RESPOD modes of forcing, respectively, onto streamwise harmonic waves with supersonic phase speeds. Different frequencies ranging from $St = 0.4$ to 1 are shown from top to bottom.

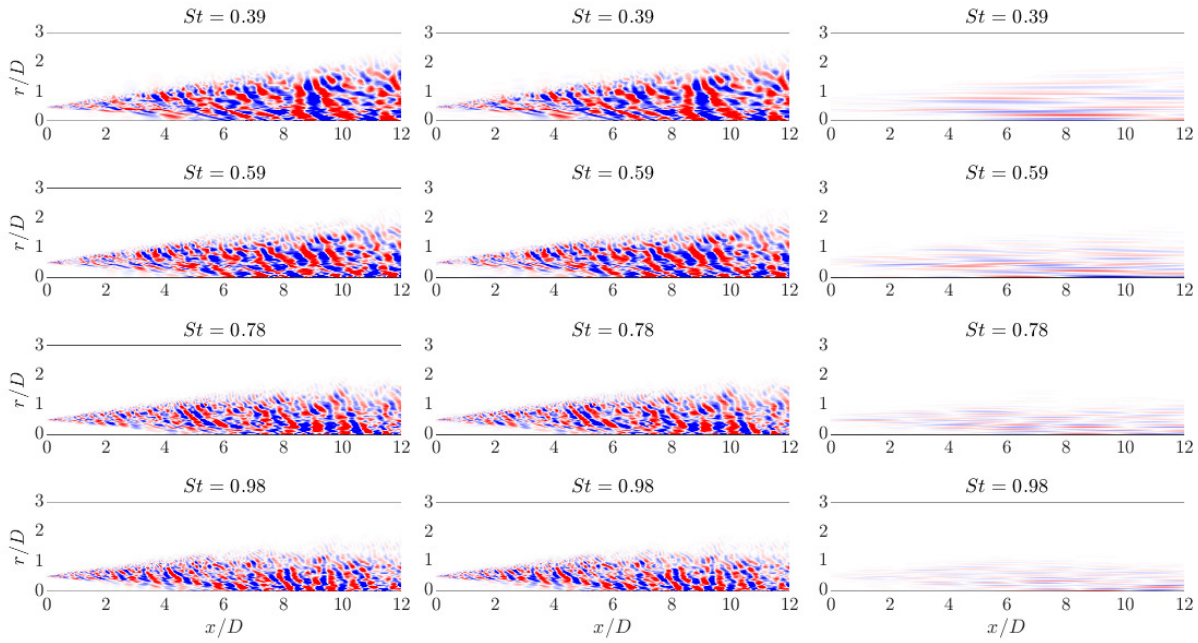

Fig. 7 Real part of the first RESPOD mode of forcing (left) compared to its subsonic (middle) and supersonic (right) parts. Different frequencies ranging from $St = 0.4$ to 1 are shown from top to bottom.

where $L = 30D$ is the domain length, and using this FT, decompose the first RESPOD mode of forcing, $\boldsymbol{\chi}^{(1)}$ into two parts, $\boldsymbol{\chi}^{(1-)}$ and $\boldsymbol{\chi}^{(1+)}$, containing subsonic and supersonic components, respectively [32]. The resulting forcing fields are depicted in comparison to the original forcing mode in figure 7. It is seen that most of the forcing energy is contained in the subsonic part of the mode, $\boldsymbol{\chi}^{(1-)}$, making it indistinguishable from $\boldsymbol{\chi}^{(1)}$. The supersonic component, $\boldsymbol{\chi}^{(1+)}$, takes the form of a compilation of radially thin wavepackets with a disorganised radial phase structure.

The acoustic response generated by these subsonic and supersonic modes, $\boldsymbol{\chi}^{(1-)}$ and $\boldsymbol{\chi}^{(1+)}$, respectively, are compared to the response of the first RESPOD mode of forcing, $\boldsymbol{\chi}^{(1)}$, in figure 8 at a range of frequencies. We see that supersonic modes dominate sound generation at all frequencies and removing them leads to more than an order-of-magnitude reduction in the acoustic pressure. The energy contained in supersonic part of the RESPOD modes of forcing is shown in figure 9 for different mode numbers and frequencies. It is seen that in all the modes and frequencies, the supersonic components contain less than 5% of the mode energy. Note that the first RESPOD mode of forcing already contains less than 1% of the total forcing energy, which means that the energy fraction of the supersonic part of the first RESPOD mode of forcing, $\boldsymbol{\chi}^{(1+)}$, with respect to the total forcing energy at the same frequency, is ~0.04%, while it generates ~ 75% of the total acoustic energy in the downstream region for a frequency range, $St = [0.4, 1.0]$ at $M_j = 0.4$.

V. Conclusion

We discussed a methodology for identification of source of subsonic jet noise at low propagation angles, which we referred to as downstream noise. Since noise generation by turbulent flows is nonlinear, it is not possible to uniquely define the source terms, i.e., one can not separate the generation of the acoustic and hydrodynamic fluctuations. In any attempt to achieve this, as in the so-called acoustic analogies (Lighthill [1], Lilley [4], Howe [5], Doak [6], Goldstein [7]; etc.), one needs to assume a linear operator for the propagation of sound waves, and recast Navier-Stokes (N-S) equations accordingly. All the nonlinear terms remain after this recasting are named as *source* terms. In this study, we adopted the resolvent framework, where the mean flow is used as the linear operator, and the nonlinear terms remaining after linearisation of the N-S equations around the mean flow are seen as the source terms, or *forcing* in resolvent terminology.

Using the resolvent framework, we showed that downstream noise is generated mainly by the forcing term

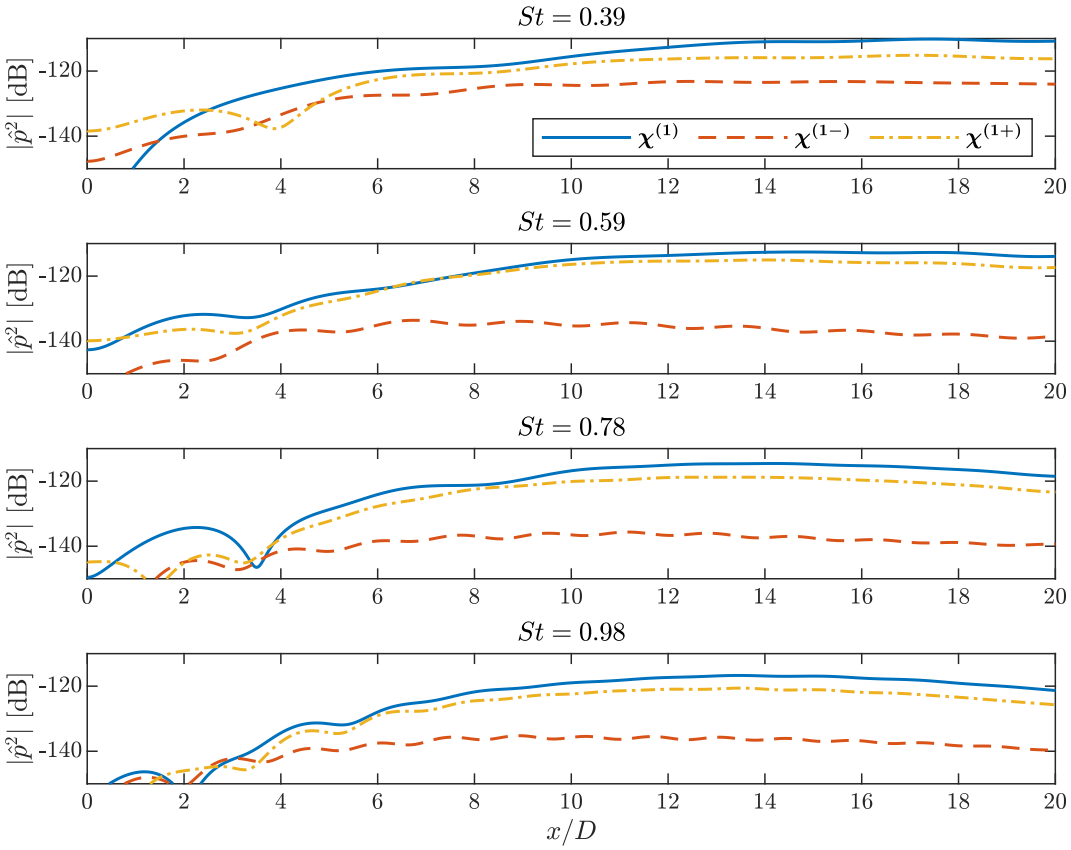

Fig. 8 PSD of the acoustic pressure generated by the first RESPOD mode of forcing (solid) compared to its subsonic (dashed) and supersonic (dash-dotted) parts. Different frequencies ranging from $St = 0.4$ to 1 are shown from top to bottom.

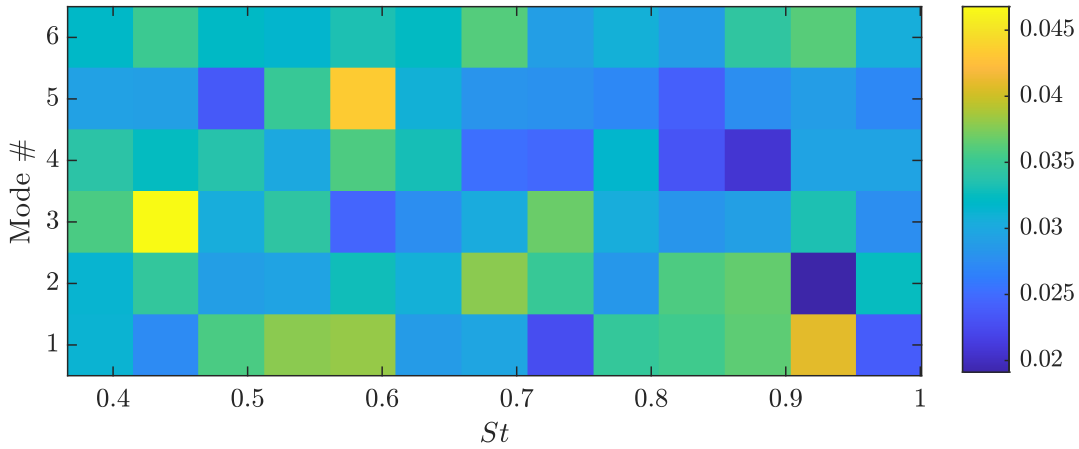

Fig. 9 Energy ratio of the supersonic part of the RESPOD mode of forcing.

corresponding to the streamwise velocity. We then obtained a low-rank reconstruction of this forcing term using the RESPOD method [18]. The RESPOD method yields forcing modes that generates the SPOD modes of the measured response, which is determined as the acoustic pressure in this study. The response modes are orthogonal to each other by construction. Searching for a similar orthogonality on the forcing side, we projected the RESPOD modes of the forcing onto streamwise harmonic waves with different phase velocities varying in the supersonic range, which yielded two critical outcomes: (*i*) projection coefficients corresponding to the first RESPOD mode of forcing peaked around the same phase velocity at all the frequencies investigated; (*ii*) projection coefficients corresponding to the second RESPOD mode of forcing showed a deep around the same phase velocity as a trace of the orthogonality in the response. Decomposing the first RESPOD mode of forcing into supersonic and subsonic components, we demonstrated that it is the supersonic part of the forcing which generates the majority of the sound field in the downstream region.

The energy ratio of supersonic part of the first RESPOD forcing mode to the entire forcing data is found to be extremely small ($\sim$0.04%), showing the importance of such an identification procedure prior to any modelling effort. The findings of this study will later be used to develop a source model to predict downstream noise in round isothermal turbulent jets. The study will be extended to include Mach number and flight effects.

Acknowledgments

This work has received funding from the Clean Sky 2 Joint Undertaking under the European Union's Horizon 2020 research and innovation programme under grant agreement No 785303. U.K. has received funding from TUBITAK 2236 Co-funded Brain Circulation Scheme 2 (Project No: 121C061).

References

[1] Lighthill, M. J., "On sound generated aerodynamically I. General theory," *Proceedings of the Royal Society of London. Series A. Mathematical and Physical Sciences*, Vol. 211, No. 1107, 1952, pp. 564–587. https://doi.org/10.1098/rspa.1952.0060.

[2] Powell, A., "Theory of Vortex Sound," *The Journal of the Acoustical Society of America*, Vol. 36, No. 1, 1964, pp. 177–195. https://doi.org/10.1121/1.1918931, URL https://doi.org/10.1121/1.1918931.

[3] Phillips, O. M., "On the generation of sound by supersonic turbulent shear layers," *Journal of Fluid Mechanics*, Vol. 9, No. 1, 1960, p. 1–28. https://doi.org/10.1017/S0022112060000888.

[4] Lilley, G. M., "On the noise from jets," *AGARD CP-131*, 1974, pp. 13–1.

[5] Howe, M. S., "Contributions to the theory of aerodynamic sound, with application to excess jet noise and the theory of the flute," *Journal of Fluid Mechanics*, Vol. 71, No. 4, 1975, p. 625–673. https://doi.org/10.1017/S0022112075002777.

[6] Doak, P. E., "Fluctuating total enthalpy as a generalized acoustic field," *Acoustical Physics*, Vol. 41, 1995, pp. 677–685.

[7] Goldstein, M. E., "A generalized acoustic analogy," *Journal of Fluid Mechanics*, Vol. 488, 2003, p. 315–333. https://doi.org/10.1017/S0022112003004890.

[8] McKeon, B. J., and Sharma, A. S., "A critical-layer framework for turbulent pipe flow," *Journal of Fluid Mechanics*, Vol. 658, 2010, pp. 336–382. https://doi.org/10.1017/S002211201000176X.

[9] Hwang, Y., and Cossu, C., "Amplification of coherent streaks in the turbulent Couette flow: an input–output analysis at low Reynolds number," *Journal of Fluid Mechanics*, Vol. 643, 2010, p. 333–348. https://doi.org/10.1017/S0022112009992151.

[10] Jordan, P., and Colonius, T., "Wave Packets and Turbulent Jet Noise," *Annual Review of Fluid Mechanics*, Vol. 45, No. 1, 2013, pp. 173–195. https://doi.org/10.1146/annurev-fluid-011212-140756.

[11] Cavalieri, A. V., Jordan, P., Agarwal, A., and Gervais, Y., "Jittering wave-packet models for subsonic jet noise," *Journal of Sound and Vibration*, Vol. 330, No. 18, 2011, pp. 4474–4492. https://doi.org/https://doi.org/10.1016/j.jsv.2011.04.007, URL https://www.sciencedirect.com/science/article/pii/S0022460X11002641.

[12] Cavalieri, A. V. G., and Agarwal, A., "Coherence decay and its impact on sound radiation by wavepackets," *Journal of Fluid Mechanics*, Vol. 748, 2014, p. 399–415. https://doi.org/10.1017/jfm.2014.186.

[13] Tam, C. K. W., Viswanathan, K., Ahuja, K. K., and Panda, J., "The sources of jet noise: experimental evidence," *Journal of Fluid Mechanics*, Vol. 615, 2008, p. 253–292. https://doi.org/10.1017/S0022112008003704.

[14] Lumley, J. L., "Toward a turbulent constitutive relation," *Journal of Fluid Mechanics*, Vol. 41, No. 2, 1970, p. 413–434. https://doi.org/10.1017/S0022112070000678.

[15] Picard, C., and Delville, J., "Pressure velocity coupling in a subsonic round jet," *International Journal of Heat and Fluid Flow*, Vol. 21, No. 3, 2000, pp. 359 – 364. https://doi.org/https://doi.org/10.1016/S0142-727X(00)00021-7, URL http://www.sciencedirect.com/science/article/pii/S0142727X00000217.

[16] Towne, A., Schmidt, O. T., and Colonius, T., "Spectral proper orthogonal decomposition and its relationship to dynamic mode decomposition and resolvent analysis," *Journal of Fluid Mechanics*, Vol. 847, 2018, p. 821–867. https://doi.org/10.1017/jfm.2018.283.

[17] Schmidt, O. T., Towne, A., Rigas, G., Colonius, T., and Brès, G. A., "Spectral analysis of jet turbulence," *Journal of Fluid Mechanics*, Vol. 855, 2018, p. 953–982. https://doi.org/10.1017/jfm.2018.675.

[18] Karban, U., Martini, E., Cavalieri, A., Lesshafft, L., and Jordan, P., "Self-similar mechanisms in wall turbulence studied using resolvent analysis," *Journal of Fluid Mechanics*, Vol. 939, 2022, p. A36. https://doi.org/10.1017/jfm.2022.225.

[19] Ffowcs Williams, J. E., "The noise from turbulence convected at high speed," *Philosophical Transactions of the Royal Society of London. Series A, Mathematical and Physical Sciences*, Vol. 255, No. 1061, 1963, pp. 469–503. https://doi.org/10.1098/rsta.1963.0010, URL https://royalsocietypublishing.org/doi/abs/10.1098/rsta.1963.0010.

[20] Crighton, D., "Basic principles of aerodynamic noise generation," *Progress in Aerospace Sciences*, Vol. 16, No. 1, 1975, pp. 31–96. https://doi.org/https://doi.org/10.1016/0376-0421(75)90010-X, URL https://www.sciencedirect.com/science/article/pii/037604217590010X.

[21] Cavalieri, A. V. G., Jordan, P., and Lesshafft, L., "Wave-Packet Models for Jet Dynamics and Sound Radiation," *Applied Mechanics Reviews*, Vol. 71, No. 2, 2019. https://doi.org/10.1115/1.4042736, 020802.

[22] Borée, J., "Extended proper orthogonal decomposition: a tool to analyse correlated events in turbulent flows," *Experiments in fluids*, Vol. 35, No. 2, 2003, pp. 188–192.

[23] Towne, A., Colonius, T., Jordan, P., Cavalieri, A. V., and Brès, G. A., *Stochastic and nonlinear forcing of wavepackets in a Mach 0.9 jet*, 2015. https://doi.org/10.2514/6.2015-2217.

[24] Brès, G., Ham, F., Nichols, J., and Lele, S., "Unstructured large-eddy simulations of supersonic jets," *AIAA Journal*, Vol. 55, No. 4, 2017, pp. 1164–1184. https://doi.org/10.2514/1.J055084.

[25] Brès, G. A., Jordan, P., Jaunet, V., Le Rallic, M., Cavalieri, A. V. G., Towne, A., Lele, S. K., Colonius, T., and Schmidt, O. T., "Importance of the nozzle-exit boundary-layer state in subsonic turbulent jets," *Journal of Fluid Mechanics*, Vol. 851, 2018, p. 83–124. https://doi.org/10.1017/jfm.2018.476.

[26] Towne, A., "Advancements in Jet Turbulence and Noise Modeling: Accurate One-Way Solutions and Empirical Evaluation of the Nonlinear Forcing of Wavepackets," Ph.D. thesis, California Institute of Technology, 2016.

[27] Martini, E., Cavalieri, A. V., Jordan, P., and Lesshafft, L., "Accurate Frequency Domain Identification of ODEs with Arbitrary Signals," *arXiv: Signal Processing*, 2019.

[28] Bugeat, B., Chassaing, J.-C., Robinet, J.-C., and Sagaut, P., "3D global optimal forcing and response of the supersonic boundary layer," *Journal of Computational Physics*, Vol. 398, 2019, p. 108888.

[29] Balay, S., Gropp, W. D., McInnes, L. C., and Smith, B. F., "Efficient Management of Parallelism in Object Oriented Numerical Software Libraries," *Modern Software Tools in Scientific Computing*, Birkhäuser Press, 1997, pp. 163–202.

[30] Freund, J. B., "Noise sources in a low-Reynolds-number turbulent jet at Mach 0.9," *Journal of Fluid Mechanics*, Vol. 438, 2001, p. 277–305. https://doi.org/10.1017/S0022112001004414.

[31] Cavalieri, A. V. G., Jordan, P., Colonius, T., and Gervais, Y., "Axisymmetric superdirectivity in subsonic jets," *Journal of Fluid Mechanics*, Vol. 704, 2012, p. 388–420. https://doi.org/10.1017/jfm.2012.247.

[32] Sinayoko, S., Agarwal, A., and HU, Z., "Flow decomposition and aerodynamic sound generation," *Journal of Fluid Mechanics*, Vol. 668, 2011, p. 335–350. https://doi.org/10.1017/S0022112010004672.